ACS APPLIED POLYMER MATERIALS

pubs.acs.org/acsapm Article

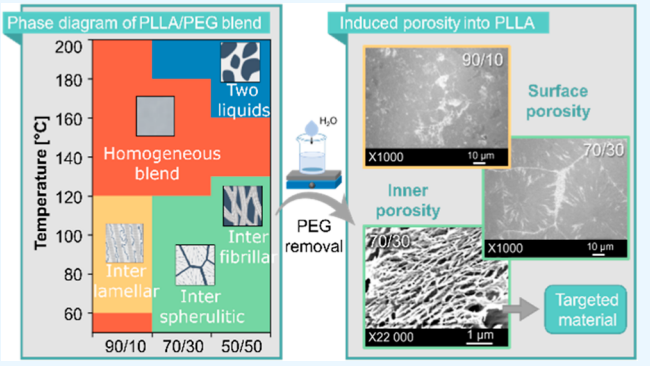
Phase Diagram of Semicrystalline Blends of Poly(L-lactic acid) and Poly(ethylene glycol)

Quentin Papeloer,* Pascal Van Velthem, Sophie Demoustier-Champagne, and Alain M. Jonas

Cite This: ACS Appl. Polym. Mater. 2024, 6, 9160−9169 Read Online

ACCESS | Metrics & More | Article Recommendations | Supporting Information

ABSTRACT: Porosity plays a critical role in determining the performance and functionality of various materials, particularly in biomedical applications where multiscale porosity is needed. This article focuses on the semimiscible nature of poly(L-lactic acid) (PLLA) and poly(ethylene glycol) (PEG) and how it can be used to induce microporosity into the PLLA after PEG dissolution. The elaboration of phase diagrams of PLLA/PEG blends was achieved by using flash differential scanning calorimetry depending on the composition of the blends and the molar mass of PEG. This analysis reveals four distinct behaviors corresponding to different temperature ranges. Above the crystallization temperature of PLLA, a homogeneous blend is observed when the PEG content is low (type I), while a higher PEG content and higher molar mass lead to liquid−liquid phase separation (type IV). Conversely, at lower temperatures, two different liquid−solid phase separations occurred due to PLLA crystallization. In blends with lower PEG content, PEG segregates within interlamellar areas (type II), whereas at higher PEG content, it accumulates within interspherulitic and interfibrillar regions (type III). The microstructural characterization of the blend by scanning electron microscopy, after PEG removal, reveals that homogeneous microporosity is achieved into PLLA spherulites whereas larger pores are obtained in the interspherulitic regions. These results are closely correlated with those obtained in the phase separation study and show that the porosity of PLLA, created after the removal of the sacrificial PEG, can effectively be modulated by tuning the miscibility of the different components in the blend material. Moreover, this method allows us to induce porosity after shaping the material. Therefore, it can be combined with other polymer processing techniques, such as 3D-printing, to introduce multiscale porosity within complex objects, offering particularly interesting prospects in biomedical engineering.



KEYWORDS: *poly(lactic acid), poly(ethylene glycol), polymer blends, phase diagram, flash DSC*

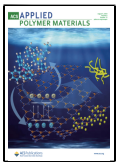
Downloaded via UNIV CATHOLIQUE DE LOUVAIN on August 9, 2024 at 11:20:07 (UTC).
See https://pubs.acs.org/sharingguidelines for options on how to legitimately share published articles.

INTRODUCTION

Porous materials with hierarchical structures are abundant in nature, e.g., wood, sponges, or coral reefs and in the human body, e.g., bones or lungs. However, they are difficult to synthesize in a controlled way due to their complex intricate shape. The significance of interconnected porous structures lies in facilitating effective diffusion within a material and amplifying the available surface area within a defined volume.[1−3] These properties are important in a variety of fields, including tissue engineering, filtration, and catalysis. Specifically, in cellular scaffolds, the precise control of porosity may enhance cell adhesion and proliferation while ensuring optimal transport within the material.[4] Porosity indeed constitutes a crucial attribute for tissue regeneration, as it allows the cells and vital substances to spread through the material. Several methods are employed for crafting porous polymer matrices, with the most prevalent being solvent extraction, electrospinning, gas foaming, and particulate leaching.[3] These techniques collectively contribute to the creation of porous structures, offering tailored solutions for diverse applications but often with limited control over the different levels of porosity.

In this context, polymer blends offer an opportunity to tune a porosity at the microscopic level by using one of the polymers as a sacrificial material. Indeed, changing the miscibility between constituent polymers can trigger phase separation in the blends, allowing the extraction of the sacrificial material and resulting in a porous structure. The advantage of this methodology is that phase separation can be controlled to a great extent from the knowledge of the phase diagram of the blend. In the context of biocompatible hierarchic porous structures, poly(lactic acid) (PLA) and poly(ethylene glycol) (PEG) blends come naturally as good

Received: May 16, 2024
Revised: July 12, 2024
Accepted: July 14, 2024
Published: July 24, 2024



ACS Publications © 2024 American Chemical Society

candidates, fulfilling all of the essential criteria for targeted application. Indeed, they are both biocompatible and are already widely used in the biomedical sector, and PLA is biodegradable.[4,5] Additionally, the water solubility of PEG makes it an ideal sacrificial material, as it can be extracted without the need of organic solvents. Also, as both of them exhibit semicrystalline behavior, phase separation can be triggered either in the liquid phase by a liquid−liquid phase separation as in classical amorphous polymer blends or by the crystallization of one of the components in a liquid−solid phase separation process.[6,7]

In the past decades, PEG was used with PLA added as the plastifying agent to tune PLA properties. Therefore, to better understand the interactions between those two polymers, their crystallization and miscibility were studied. The semimiscible nature of PLA and PEG was demonstrated by Younes and Cohn.[8] Below 30 wt % PEG in the blend, the polymers form a homogeneous phase in the liquid phase. However, when increasing the PEG content above this threshold, each polymer crystallizes individually upon cooling, and liquid−solid phase separation occurs. This observation was subsequently supported by other studies, even if the threshold for the observation of liquid−solid phase separation varies from a PEG weight ratio of 10 to 50% depending on conditions.[9−12] In a later study, Nakafuku and Sakoda investigated more thoroughly the crystallization of PLA in the presence of PEG.[12] They showed that even if PEG strongly influences PLA crystallization, both polymers crystallize separately with no cocrystallization as expected given the crystallographic differences between the two unit cells. The addition of PEG below the phase separation threshold has been shown to enhance PLA crystallinity and flexibility, due to the plasticization by PEG of the amorphous regions in the semicrystalline microstructure of PLA.[10−14] This effect is however reduced when the PEG molar mass increases from 2 to 5000 kDa.[13] Moreover, it appears that the presence of PEG increases the spherulitic growth rate of PLA and leads to the formation of banded spherulites.[14] This comes from constraints on the growing PLA lamellae resulting from the nearby presence of PEG rejected in the amorphous PLA regions. In addition to its influence on the physical properties of PLA, the incorporation of PEG offers other notable advantages. For instance, it has been shown that PEG increases both hydrolytic[10] and enzymatic, degradation[10,15,16] rate of PLA. The degradation rate was mostly increased due to the porosity induced by the dissolution of PEG into water, increasing the surface area available for enzymatic attack.

The phase separation phenomenon between PLA and PEG offers interesting opportunities to achieve a porous material by selectively removing PEG from the PLA matrix; depending on the scale of the phase separation, a variety of pore sizes can be obtained. Various techniques were used to induce the porosity within PLA/PEG blends. One of the simplest methods consists of extracting PEG from the blend with water.[17,18] It was observed that the pore size increases with escalating PEG molar masses from 1 to 100 kDa and PEG ratios from 20 to 80 wt %, with pore sizes ranging from a few micrometers to several hundred micrometers. By using the same technique, channelized pores[18] and multiscale porosity were also achieved.[19] Notably, particulate leaching, employing salt particles embedded in pure PLA[20] and PCL/PEG 50/50 blends,[21] has also proven effective in generating multiscale porosity. Following water extraction, larger and smaller pores are obtained from the corresponding sites previously occupied by salt particles and PEG within the blend, respectively. Despite this work, the interplay between PLA crystallization, phase separation, and porosity after extraction of PEG remains unclear, in part because a complete understanding of the PLA/PEG phase diagram is still lacking. Liquid/liquid phase separation of PLA and PEG was already studied by differential scanning calorimetry (DSC), revealing the presence of different glass transition temperatures (T_g) attesting the presence of different phases.[22] Although this method works well for amorphous blends, T_g becomes less visible when the polymers crystallize, making it impossible to link phase diagram and crystallization.

In this study, particular attention is given to constructing a comprehensive phase diagram for PLA/PEG blends across a wide range of temperatures. The use of flash DSC (fDSC) with extremely rapid cooling rates provides the ability to quench samples instantaneously and capture snapshots of the blend state without the perturbation of (re)crystallization during cooling and subsequent heating. This approach is crucial for examining temperatures that are typically inaccessible due to rearrangement during heating. As a result, a phase diagram incorporating crystallization can be developed. This sheds light on various factors influencing phase separation and facilitates determination of the location of PEG within the blend. This information already enables prediction of the material porosity after PEG extraction. Subsequently, the study delves into investigating the induced porosity of the material through scanning electron microscopy (SEM) analysis, conducted after the selective removal of PEG. This approach elucidates the PEG location within the blend across various scales and can be related to the previously established phase diagram. Finally, the impact of the PEG molar mass on phase separation, crystallization behavior, and the resulting porosity is explored through a combination of fDSC and SEM analysis. These objectives contribute to a deeper understanding of PLA and PEG blends in material design, offering potential avenues for advancement in biomedical applications.

MATERIALS AND METHODS

Materials. The poly(L-lactic acid) (PLLA) used in this work is Ingeo 2500HP in pellet form from NatureWorks. Its weight-average molar mass (M_w) is reported to be around 10^5 g/mol with a dispersity of 1.7. PEG powder with a M_w of 3350 g/mol (PEG 3K), 100,000 g/mol (PEG 100K), and 1,000,000 g/mol (PEG 1M) was purchased from Sigma-Aldrich. Chloroform ($CHCl_3$) was also purchased from Sigma-Aldrich and used as received.

Sample Preparation. *Production of PLLA/PEG Films by Solvent Casting.* PLLA pellets and PEG powder were dried overnight at 40 °C under a vacuum before processing. PLLA/PEG blends with different compositions (10, 30, and 50 PEG wt %) were dissolved in $CHCl_3$ to obtain a total polymer concentration of 40 mg/mL. The vials were then hermetically closed to prevent evaporation of the solvent. The solutions were magnetically stirred until the obtention of a homogeneous transparent liquid and further cast on glass Petri dishes. The solvent was removed by evaporation overnight at room temperature. The thickness of the films was measured with a micrometer and was around 30 μm.

Crystallization of PLLA/PEG Films Using the Hot Pressing Method. Before use, PLLA/PEG films were dried overnight at 40 °C under a vacuum. Dried films were then sandwiched between two metallic plates covered with Kapton and submitted to isothermal crystallization at 110 °C. A thick aluminum foil was cut and used as a template to obtain samples of 5 mm × 5 mm. To eliminate the thermal history, these blend assemblies were first put in a hot press at

https://doi.org/10.1021/acsapm.4c01509
ACS Appl. Polym. Mater. 2024, 6, 9160−9169

200 °C for 5 min and further placed into a second hot press at 110 °C for 4 h to favor crystallization. Minimal pressure was applied to allow good contact on both faces of the samples. At the end, PLLA/PEG films were quenched in air from 110 °C to room temperature.

Extraction of PEG. For PEG extraction, the isothermally crystallized PLLA/PEG blends were immersed into distilled water at room temperature for 1 h. This process was repeated twice, and then the samples were immersed one last time into distilled water for 24 h. The water was replaced between each step to eliminate the dissolved PEG.

Characterization Techniques. *fDSC Analysis.* fDSC analysis was used to measure the glass transitions of the blends ($T_{g,blend}$) and to investigate the isothermal crystallization of the blends at different temperatures. fDSC experiments were carried out with a flash-DSC1 instrument from Mettler Toledo connected to an intracooler and N_2 purge gas. Before analysis, PLLA/PEG films were dried overnight at 40 °C under vacuum. Then, a small piece of the films (ca. a few hundreds of nanograms) was cut with a razor blade and manipulated with a paintbrush hair under microscope. The fDSC samples were too small for their mass to be measured. The samples were then placed in the center of the fDSC chip. The temperature ramps used in fDSC are described in Figure 1. Initially, the thermal history of all samples was

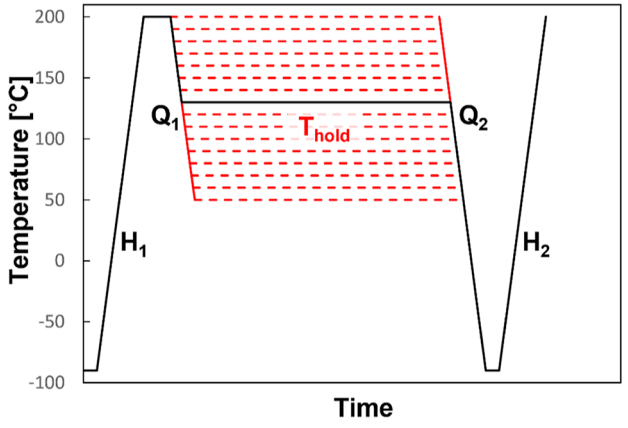


Figure 1. fDSC temperature ramps used to determine the phase diagram of PLLA/PEG blends.

erased by first heating (H_1) at 1000 K/s. Subsequently, samples were held at 200 °C, above the melting temperature of PLLA ($T_{m,PLLA}$), for 1 s to eliminate any residual crystals. The samples were then quenched for the first time (Q_1) at 1000 K/s from the molten state to a temperature T_{hold} at which the blend state is investigated. Samples were maintained at this temperature for 5 min to allow them to reach thermodynamic equilibrium. Indeed, results from experiments performed with different isothermal durations and different PEG molar masses, presented in Figure S1, confirm that after 5 min, equilibrium is attained. T_{hold} was varied from 200 to 50 °C for each sample to observe the evolution of the blend state in this temperature range. Once at equilibrium, the samples were submitted to a second quench (Q_2) at 1000 K/s from T_{hold} to −90 °C, effectively "freezing" their equilibrated states. This state was ultimately observed on the second heating (H_2) at 1000 K/s. The T_g as well as the melting temperature (T_m) were defined as the midpoint of the specific heat jumps and the maximum of the endothermic peaks in the fDSC curves, respectively.

SEM Analysis. The porosity induced by the removal of PEG from the blends was observed by SEM using a JEOL 7600F microscope under an acceleration voltage of 5 kV and a working distance of 8 mm. Prior to analysis, extracted films were cut with a razor blade to observe the porosity inside the material. The samples were then coated with a 12 nm layer of gold using a Ted Pella Cressington208HR High-Vacuum Turbo Sputter Coater.

RESULTS

Study of Miscibility and Crystallization of PLLA/PEG Blends by fDSC. To fully understand the behavior of PLLA/PEG blends, it is important to know the different states that PLLA and PEG can reach depending on the temperature to which they are subjected. This can be achieved by using fDSC. With its extremely rapid cooling rate, fDSC enables almost instantaneous temperature changes. Consequently, samples can be quenched from high temperature (200 °C) to low temperature (−90 °C) without allowing any reorganization, such as crystallization or cold crystallization. This approach enables the observation of sample states originating from a desired temperature.

The fDSC procedure described in Figure 1 was applied for analyzing all PLLA/PEG blend samples of three compositions (90/10, 70/30, and 50/50) with PEG of three different molar masses (3K, 100K, and 1M). The curves presented in Figure 2 illustrate the second heating curves (H_2) for samples 90/10 (a−c), 70/30 (d−f), and 50/50 (g−i) with PEG molar masses of 3K (a, d, g), 100K (b, e, h), and 1M (c, f, i). In each graph of Figure 2, T_{hold} varies from 200 °C (upper curve) to 50 °C (lower curve), with an increment of 10 °C. Since the main objective of this study is to interpret the interactions between PLLA and PEG within the blend, the principal trends observed in the fDSC curves are examined, with colors for the traces used to help the reader sort the different samples in different categories of behavior. The fDSC curves of PLLA and the ones of PEG 3K, 100K, and 1M are presented in Figures S2 and S3, respectively, in the Supporting Information. The degrees of crystallinity of the different samples are also presented in Figure S4.

In Figure 2a−c, the behavior of the 90/10 blends exhibits a consistent pattern independently of the PEG molar mass. Notably, a single T_g is observed for equilibration temperatures T_{hold} between 200 and 120 °C (red curves), whose temperature location should correspond to the one of a miscible amorphous blend according to Fox's equation.[23] The width of the specific heat jump at T_g is not large, which is indicative of the homogeneity of the blend composition at T_{hold}. For T_{hold} values between 110 and 60 °C (yellow curves), PLLA undergoes crystallization during isothermal equilibration at T_{hold}; as a result, a high-temperature endotherm is detected upon heating, corresponding to the melting of PLLA crystals, with the melting temperature ($T_{m,PLLA}$) decreasing as T_{hold} decreases (yellow curves). Additionally, a small melting endotherm of PEG crystals is observed slightly before 50 °C for the lower PEG molar mass, indicating that PEG crystallized at least partially during cooling after PLLA crystallization at T_{hold}, owing to its accumulation in PEG-rich regions due to segregation during PLLA crystallization. The downward shift of $T_{m,PLLA}$ as T_{hold} decreases is due to PLLA crystallizing at different T_{hold} temperatures, resulting in the selection of a lower average lamellar thickness and, consequently, lower melting temperature. This is qualitatively in accordance with the Hoffman−Weeks relationship,[24] although the possible depression of the melting temperature due to the presence of PEG in the amorphous regions surrounding PLLA crystals might complicate the picture. Finally, at a T_{hold} of 50 °C, the temperature is insufficient to allow PLLA crystallization, resulting in the observation of a single T_g, similar to the isotherms at higher temperatures; these fDSC traces are actually more complex but will not be discussed further.

https://doi.org/10.1021/acsapm.4c01509
ACS Appl. Polym. Mater. 2024, 6, 9160−9169

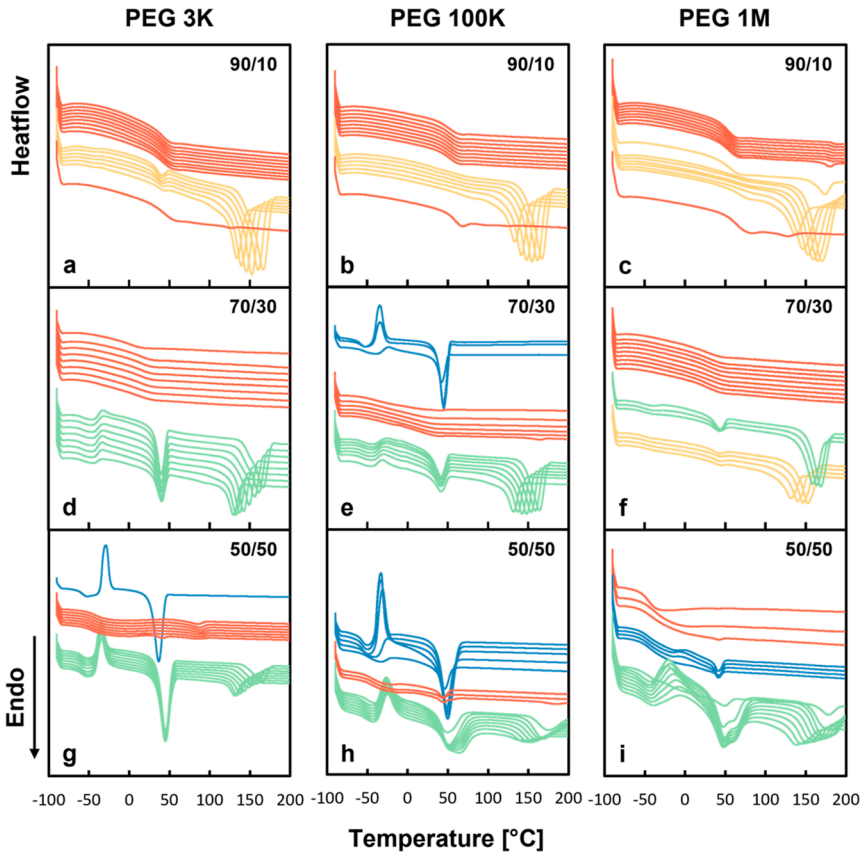


Figure 2. fDSC second heating curves (H_2) for PLLA/PEG samples 90/10 (a–c), 70/30 (d–f), and 50/50 (g–i) with T_{hold} varying from 200 to 50 °C by steps of 10 °C from top to bottom in a panel (the curves have been shifted vertically for clarity). The PEG molar mass is 3K (a,d,g), 100K (b,e,h), and 1M (c,f,i). The colors are used to identify different categories of behavior. Type I (red): miscible amorphous blend with no visible melting peak. Type II (yellow): liquid–solid phase separation driven by PLLA crystallization without PEG crystallization during the isothermal treatment. Type III (green): liquid–solid phase separation driven by PLLA crystallization with PEG crystallization during isothermal treatment. Type IV (blue): liquid–liquid phase separation.

PLLA/PEG 70/30 blends (Figure 2d–f) exhibit more diverse behavior depending on the PEG molar mass. For PEG 3K (Figure 2d), a single T_g is observed under isothermal equilibration conditions ranging from 200 to 130 °C (red curves), again testifying for the homogeneity of the amorphous blend at these temperatures; nevertheless, the width of the glass transition increases, suggesting less locally homogeneous blends. Furthermore, several thermal transitions occur during the heating following isothermal equilibration between 120 and 50 °C (green curves). These transitions appear in the following sequence: T_g of PEG ($T_{g,PEG}$), cold crystallization of PEG ($T_{cc,PEG}$), PEG melting ($T_{m,PEG}$), and $T_{m,PLLA}$. The presence of well-defined PEG transitions proves that PEG accumulates in PEG-rich regions during the equilibration of the blend at T_{hold}, due to liquid–solid phase separation induced by PLLA crystallization; the invariance of $T_{m,PEG}$ with T_{hold} results from it crystallizing upon heating from PEG-rich regions in the fDSC. Again, the downward shift of $T_{m,PLLA}$ as T_{hold} decreases is due to PLLA crystallizing at different T_{hold} temperatures as for the yellow curves in panels a–c. Of note, $T_{g,PLLA}$ is not detected on these curves, which can be attributed to two factors: reduced specific heat jump due to PLLA crystallinity and overlap with the PEG melting peak in the same temperature range.

For PEG 100K (Figure 2e), a supplementary behavior appears when T_{hold} exceeds 170 °C (blue curves). In this T_{hold} range, the PLLA melting peak is not visible, indicating that PLLA remains in an amorphous state when held above its melting temperature, which is hardly surprising. However, the observation of PEG thermal transitions, which become less prominent as temperature decreases, is indicative of a liquid–liquid phase separation in this T_{hold} range, which is stronger at higher temperatures, suggesting the presence of a lower critical solution temperature (LCST) for this specific blend. Below 170 °C, the behavior observed for the blend of lower PEG molar masses is recovered.

For PEG 1M (Figure 2f), the same behavior as for the blend with the PEG of the lower molar mass is observed for T_{hold} above 90 °C. From this point on, however, the thermal transitions of PEG become barely perceptible (yellow curves), which indicates that PEG cannot crystallize as readily in the PLLA-crystallized blend. This must be due to larger constraints set on the PEG chains, either resulting from segregation in regions of much lower size still interacting strongly with PLLA-rich regions or from incomplete segregation. Both phenomena are favored by the increased viscosity of the PEG chains of high molar masses, in qualitative agreement with predictions made in the seminal work of Keith and Padden.[7]

PLLA/PEG 50/50 blends (Figure 2g–i) exhibit the same categories of behavior as blends of lower PEG content but for different isothermal equilibration temperatures. For PEG 3K and PEG 100K, the behavior of 50/50 and 70/30 blends is very similar, with a region of liquid–liquid phase separation at high temperatures (blue curves, not detected at lower PEG

https://doi.org/10.1021/acsapm.4c01509
ACS Appl. Polym. Mater. 2024, 6, 9160–9169

contents), homogeneous composition at intermediate equilibration temperature (red curves), and liquid−solid phase separation due to PLLA crystallization at lower equilibration temperature (green curves). The T_g of the homogeneous blends is located at lower temperatures than in PLLA-richer blends, again in qualitative accordance with Fox's equation. In liquid−solid phase-separated blends, the T_g of PEG is also lower than those for other samples, which indicates that PEG accumulates in PLLA-poorer regions upon segregation. Likewise, the melting enthalpy of PEG is now significantly larger than the one of PLLA, due to the higher PEG content. Other minimal differences are observed in the behaviors of the 70/30 and 50/50 blends for PEG 100K when comparing Figure 2e,h. Although the three distinct behaviors remain consistent, the transition between them occurs at lower temperatures; for instance, the transition between blue and red curves happens at 160 °C for 50/50 blends and 180 °C for 70/30 blends.

The most intriguing behavior is exhibited by the 50/50 blend with PEG 1M (Figure 2i), for which a single sharp glass transition is observed at 200 °C, indicating miscibility in the melt; however, as the equilibration temperature decreases, the T_g broadens considerably and then the behavior of a liquid−liquid phase-separated blend emerges for T_{hold} between 170 and 140 °C, before liquid−solid phase separation starts to appear (green curves). Such a behavior is typical for the existence of an upper critical solution temperature (UCST). Finally, in the low-temperature region, two melting endotherms are detected for PEG, suggestive of the possibility that PEG crystallized in two environments, one being associated with PEG-richer regions appearing due to partial liquid−liquid phase separation and the second resulting from liquid−solid phase separation in PLLA-richer regions of the liquid−liquid phase-separated morphology.

Summing up, four different types of behavior can be distinguished depending on equilibration temperature, blend composition, and PEG molar mass: type I (red curves) corresponding to homogeneous amorphous blends in which no crystallization occurs at T_{hold}; type II (yellow curves), for which PLLA crystallizes from a homogeneous amorphous mixture resulting in liquid−solid phase separation, while PEG does not (or hardly) crystallize owing to its small concentration or constraints set by nearby PLLA crystals; type III (green curves), for which both PLLA and PEG crystallize, indicative of a liquid−solid phase separation from a homogeneous and, in some case, liquid−liquid phase-separated blend; and type IV (blue curves), for which only PEG crystallizes from PEG-rich regions created by a liquid−liquid phase separation process in the amorphous blend. To add to this complexity of behaviors, some curves exhibit hybrid states, straddling the boundaries of two distinct behaviors. Therefore, they could arguably be associated with a supplementary specific behavior. But more importantly, these hybrid curves show that the transition from one behavior to another one occurs progressively, without sudden or abrupt shifts.

Overall, the complexity of the phase diagram is astonishing, with the possible existence of two liquid−liquid phase separation processes (UCST and LCST) appearing depending on equilibration temperature and on PEG concentration and molar mass and a liquid−solid phase separation appearing afterward.

Type-I behavior is typical of a miscible blend where the $T_{g,blend}$ is located between the T_g of PLLA (332.5 K for a high molar mass and slow cooling[25]) and the T_g of PEG (206 K for a high molar mass and slow cooling[26]). This indicates that PLLA and PEG form a single liquid phase under these conditions. The glass transition of these blends at different compositions and for different molar masses is presented in Figure 3. As expected, when increasing the PEG content in the

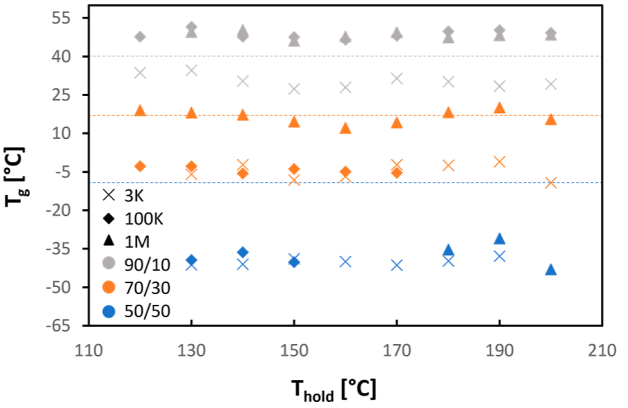


Figure 3. $T_{g,blend}$ from type-I curves in which only a single T_g is present, for noncrystallized PLLA/PEG blends of 90/10 (gray), 70/30 (orange), and 50/50 (blue) with PEG molar masses of 3K (×), 100K (◆), and 1M (▲), vs the equilibration temperature T_{hold}. Theoretical T_g's derived from Couchman's equation are represented by dotted lines in the corresponding colors.

blend, the $T_{g,blend}$ decreases significantly. The values of the glass transition temperature of a miscible blend can be estimated by Couchman's equation,[27] using the values of specific heat jump of the two polymers at T_g (38.96[26] and 42.07 J/mol/K[25] for PEG and PLLA, respectively); this equation is often simplified to give Fox's equation, which is valid when the glass transition temperatures and specific heat jumps at T_g are not too different. The $T_{g,blend}$ values computed by Couchman's equation are 40 °C for 90/10, 17 °C for 70/30, and −9 °C for 50/50. These values are only indicative, since chain end effects cannot be neglected for PEG 3K; furthermore, owing to the rapid cooling in the fDSC, kinetic effects could result in shifts of the glass transition by as much as 10 K. The $T_{g,blend}$'s measured on noncrystallized blends (Figure 3) significantly differ from the expected theoretical value; at higher PEG contents, they are generally consistently lower than the theoretical values (represented by dotted lines in Figure 3). In addition to the effects mentioned above, local fluctuations of concentrations in the blends, which are indicated by the breadth of the specific heat jump at T_g, may also contribute to the discrepancy between the expected and measured values.

The T_g's measured for the three 70/30 blends are also reported in Figure 4. For the sake of clarity, the color code remains consistent with the different behaviors displayed in Figure 2. In the low and high T_{hold} ranges, only the glass transition of almost pure PEG is detected ($T_{g,PEG}$) at ca. −50 °C, due to liquid−solid (low T_{hold}'s) or liquid−liquid (high T_{hold}'s) phase separation with the formation of almost pure PEG regions. In the intermediate range of equilibration temperatures, a glass transition temperature of a miscible blend is obtained, indicating the formation of a homogeneous mixture of PLLA and PEG, thus demonstrating miscibility. However, the onsets and offsets of the glass transition (represented by the lower and upper bars in Figure 4) indicate

https://doi.org/10.1021/acsapm.4c01509
ACS Appl. Polym. Mater. 2024, 6, 9160−9169

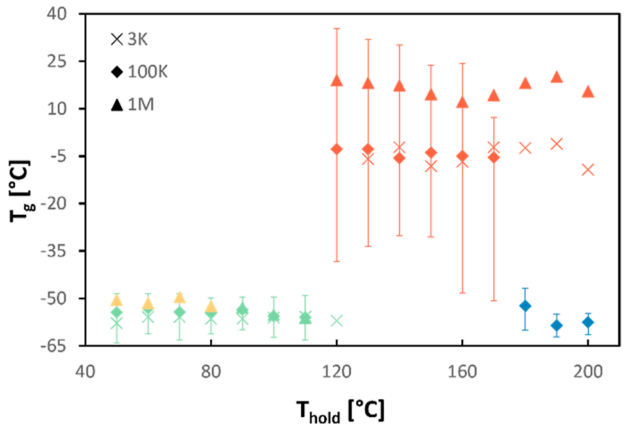


Figure 4. T_g of PLLA/PEG 70/30 blends depending on T_{hold}. The PEG molar masses are 3K (×), 100K (◆), and 1M (▲). The different colors correspond to the different types of behaviors: type I (red), II (yellow), III (green), and IV (blue). Errors bars are only shown for PEG 100K for clarity and correspond to the temperature range between the onset and offset temperatures of the specific heat jump.

a relatively heterogeneous local concentration within the blends, as previously discussed. Given that the behavior across temperature ranges is consistent regardless of the PEG molar mass, only the onset and the offset for PEG 100K are represented on the graph for more clarity.

Since crystallization occurs for type II, III, and IV behaviors, it is interesting to investigate what happens in the blend when one polymer crystallizes while the other remains in the liquid state. According to the simplified model of Keith and Padden,[7] when a polymer crystallizes into spherulites from the melt in the presence of noncrystallizable impurities, these impurities are excluded from the crystals and form an impurity-rich layer. The thickness of this layer scales as $\delta = D/G$, in which D is the diffusion coefficient of impurities in the melt and G represents the radial growth rate of the spherulites. Consequently, if D is large compared to G, a significant proportion of impurities is expelled from the spherulites, resulting in a large δ. Conversely, when G is large compared to D, the crystallization occurs too fast to expel all of the impurities out of the spherulites. As a result, δ becomes small, and most impurities remain trapped within the spherulites, which can occur either interfibrillarly when impurities form rather pure channels located between stacks of crystalline lamellae (so-called fibrils) or interlamellarly when it accumulates in the amorphous interlamellar regions of the crystallizing polymer in coexistence with amorphous segments of this polymer (tie molecules, loose folds, sharp folds, dangling chain ends, etc.).[28] This is in accordance with the PEG extraction results, presented in Figure S5, revealing that around 8% of PEG remains in the samples after extraction, most probably due to its trapping in interlamellar regions.

When PLLA crystallizes during the equilibration isotherms, the PEG chains act as impurities. A proportion of them will thus be expelled interspherulitically while the remaining part will be trapped intraspherulitically either in interfibrillar or interlamellar regions, depending on the D/G ratio. In type-II behavior (yellow curves), only PLLA crystallizes, with no PEG crystallization detected upon reheating. This behavior mainly appears for 90/10 blends in which the PEG concentration is low. The PEG-rich zones, resulting from the exclusion of PEG or its entrapment within the spherulites, are too small and/or not pure enough to allow PEG crystallization. This suggests that the liquid−solid phase separation triggered by PLLA crystallization results in interlamellar segregation of PEG, or possibly interfibrillar segregation in very small pockets in the spherulitic microstructure of PLLA. In type-III behavior (green curves), PLLA crystallizes during the isothermal equilibration, whereas PEG crystallizes upon heating. During PLLA crystallization at T_{hold}, PEG is thus expelled out of the growing PLLA crystals (liquid−solid phase separation) and accumulates to form PEG-rich areas, either in interspherulitic or interfibrillar regions. This behavior appears for all 70/30 and 50/50 blends. At those concentrations, PEG thus forms pockets within the PLLA crystalline microstructure that are large enough to crystallize. Finally, for type-IV behavior (blue curves), only PEG crystallizes during heating after equilibra-

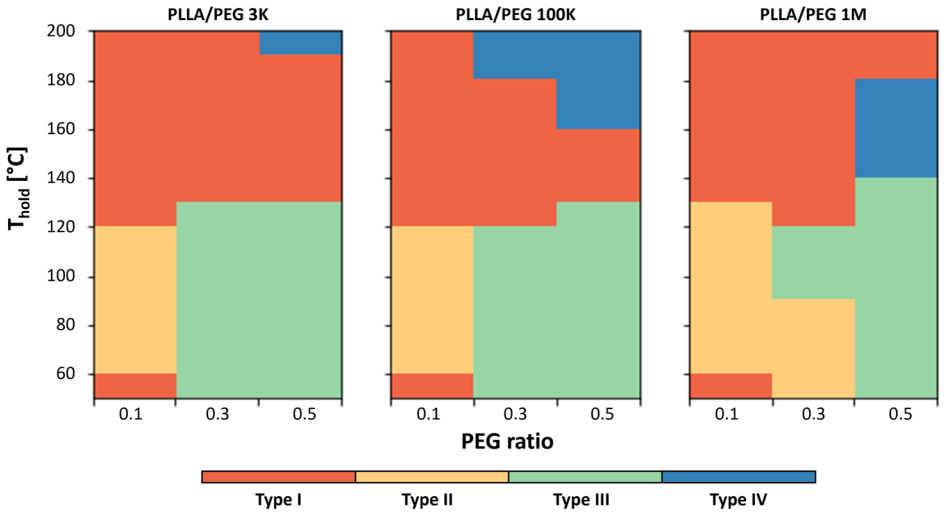


Figure 5. Temperature−concentration phase diagrams of PLLA/PEG blends based on the four types of behaviors obtained by fDSC for PEG 3K (left), PLLA/PEG 100K (center), and PLLA/PEG 1M (right). Type I: miscible blends. Type II: liquid−solid phase separation driven by PLLA crystallization with PEG segregation in interlamellar PLLA/PEG regions. Type III: liquid−solid phase separation driven by PLLA crystallization with PEG segregation in interspherulitic and/or interfibrillar regions. Type IV: liquid−liquid phase separation.

https://doi.org/10.1021/acsapm.4c01509
ACS Appl. Polym. Mater. 2024, 6, 9160−9169

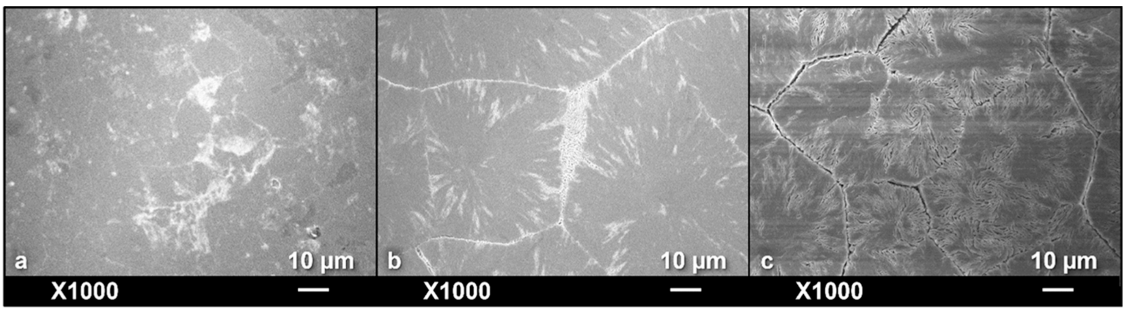


Figure 6. SEM images of the surface of films of the PLLA/PEG 3K blend crystallized for 4 h at 110 °C, after PEG extraction. The composition of the blend before extraction is 90/10 (a), 70/30 (b), and 50/50 (c).

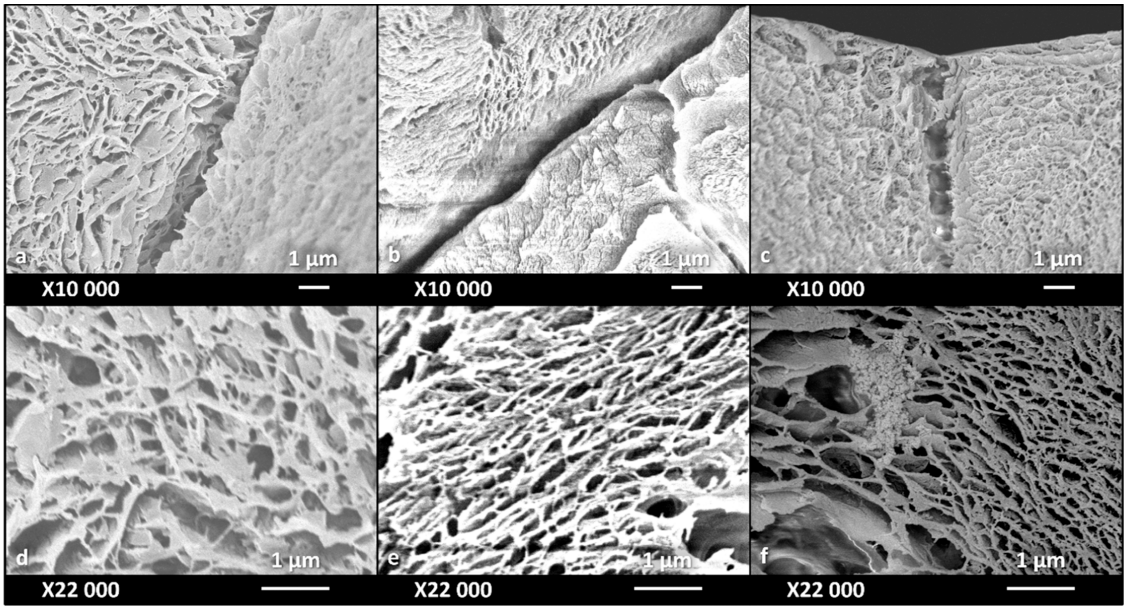


Figure 7. SEM images of the PLLA/PEG 70/30 blend after PEG dissolution. The PEG molar mass used before extraction was 3K (a,e), 100K (b,d), and 1M (c,f). The upper line shows the interspherulitic porosity whereas the lower line shows the intraspherulitic porosity.

tion, as evidenced by the presence of its cold crystallization peak. This behavior is mostly observed at high T_{hold}'s indicating that during the isothermal treatment, PLLA and PEG underwent liquid−liquid phase separation.

It is important to note that Keith and Padden's theory aids in understanding the various behaviors observed in the blend. However, the fDSC curves alone do not provide a fully nonambiguous evidence to determine the position of the PEG within the PLLA. Another technique allowing observation of sample morphology is required. Results obtained by SEM will be presented in a subsequent section to support these hypotheses.

Complete PLLA/PEG Phase Diagram. Based on the fDSC analysis described in the previous section, it is possible to draw temperature−concentration phase diagrams for the PLLA/PEG blends of different PEG molar masses. These phase diagrams are presented in Figure 5 as color maps corresponding to the different behaviors of the blend using the same color code as before. The phase diagram for PEG 3K is on the left, the one for PEG 100K is in the middle, and the one for PEG 1M is on the right. In this figure, two regimes common to all three phase diagrams are discernible.

For high temperatures above 120−140 °C, PLLA does not crystallize during equilibration (red and blue, corresponding to behavior types I and IV). In this temperature regime, PEG is miscible with PLLA at low concentrations; a liquid−liquid phase separation appears at higher concentrations with an LCST clearly visible. For the high molar mass PEG, however, a UCST also seems to exist at higher temperatures. For lower temperatures, liquid−solid phase separation happens following PLLA crystallization, with large regions of pure PEG appearing above 30% PEG (behavior types II and III). Remarkably, PLLA is capable of crystallizing at isotherms ranging from 120 to 60 °C, down to ca. 10 °C below its T_g. This plasticizing effect can be attributed to the presence of PEG, which increases chain mobility and reduces $T_{g,PLLA}$ upon mixing, allowing crystallization at lower temperatures.

Induced Porosity by PEG Extraction from PLLA/PEG Blends. In addition to providing insights into the interactions between PLLA and PEG within the blend, studying the phase diagram between PLLA and PEG enables the prediction of the PLLA porosity after PEG extraction. By selecting a PEG solvent that is a nonsolvent for PLLA, it is possible to selectively dissolve PEG. Pores or cavities then result from the local removal of PEG.

To this aim, PLLA/PEG blends of different compositions and containing PEG of different molar masses were melted and quenched to 110 °C, a temperature at which liquid−solid phase separation occurs due to the crystallization of PLLA (types II and III). The blends were held for 4 h before being

https://doi.org/10.1021/acsapm.4c01509
ACS Appl. Polym. Mater. 2024, 6, 9160−9169

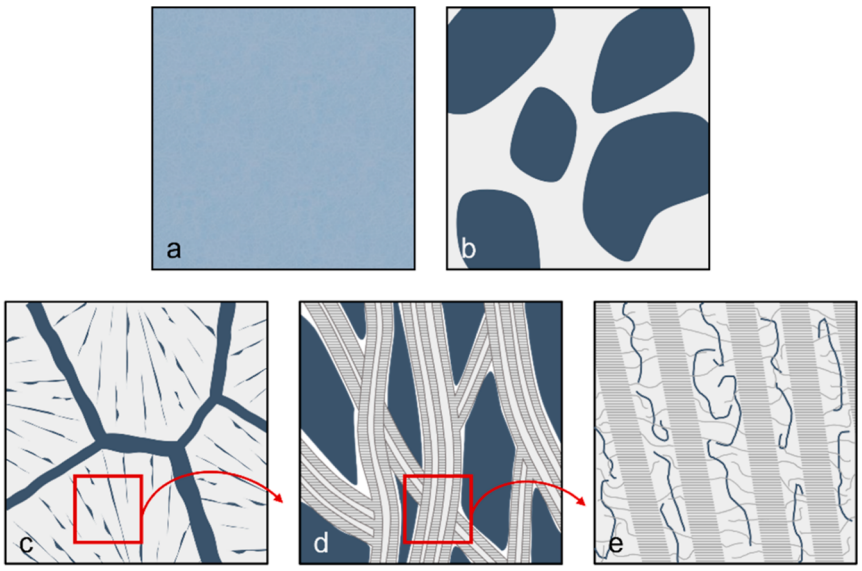


Figure 8. Various positions of PEG (blue) mixed with PLLA (gray). In the liquid phase: homogeneous blend (a) or heterogeneous blend (b) corresponding to red and blue regions of the phase diagram of Figure 5, respectively. In the solid phase, corresponding to yellow and green regions of the phase diagram: PEG located in interspherulitic regions (c), interfibrillar regions (d), and interlamellar regions (e). The proportion between the different types of PEG segregation depends on the concentration and molar mass of PEG, with lower molar masses and higher concentrations favoring interspherulitic and interfibrillar segregation.

quenched to room temperature to freeze the microstructure. Subsequently, PEG was extracted with distilled water, and the porous films were dried before analysis.

To analyze the impact of the composition on the resulting sample morphology, the surfaces of the films were first observed by SEM [Figure 6, for PLLA/PEG 3K 90/10 (a), 70/30 (b), and 50/50 (c)]. In Figure 6a, white areas corresponding to the original location of the PEG before extraction are visible. These areas are relatively small and distributed throughout the material, in accordance with type-II behavior (no large PEG regions in the microstructure). With increasing PEG concentration within the blend, there is an accumulation of PEG at the PLLA spherulite interfaces, along with larger PEG-rich regions within them, corresponding to type-III behavior. As discussed in the previous section, a proportion of PEG is trapped within PLLA spherulites, while another part is excluded, residing in the interspherulitic regions. This is precisely what is observed in Figure 6b,c for the 70/30 and 50/50 blends. Additionally, intraspherulitic PEG zones exhibit an elongated radial appearance, indicating their entrapment between lamellar stacks (fibrils). The 70/30 and 50/50 blends exhibit similar characteristics with these features becoming more pronounced with increasing PEG concentration. For the higher PEG content, accumulation of PEG in interspherulitic regions even leads to a spherulite disjunction and material decohesion. Accordingly, the PLLA/PEG 50/50 samples were particularly brittle after the PEG extraction.

Based on these results, the 70/30 samples emerged as the most promising candidates for combining porosity and mechanical properties as 90/10 blends are not porous enough and 50/50 blends are too fragile. On these samples, the porosity after PEG removal was thus studied over the entire film thickness rather than on film surfaces [Figure 7, for PEG 3K (a, d), 100K (b, e), and 1M (c, f)]. As expected, all films showed the porosity associated with the extraction of larger PEG-rich regions. The top row samples (Figure 7a–c) display interspherulitic porosity vs the PEG molar mass; the interspherulitic porosity is stronger for the lower PEG molar masses. Due to its larger molar mass, PEG 1M is less readily expulsed (smaller diffusion coefficient D) and tends to segregate predominantly in intraspherulitic regions. On the bottom row (Figure 7d–f), intraspherulitic porosity is depicted. A very similar open porosity is evident across all samples. The elongated appearance of pores is consistent with PEG entrapment during PLLA crystallization. It is also noteworthy that pore sizes range from 0.5 to 1.5 μm as also found by Lai[29] that produced porous PLLA/PEG films with a similar morphology. Although below 100 μm, which is the minimal pore size for cell migration,[2] the widespread porosity throughout the material could facilitate the diffusion of nutrients, oxygen, and other elements transported within a fluid. Those results also show that for a constant PEG content, decreasing the PEG molar mass can increase the proportion of PEG expulsed from the spherulites. This can allow us to change the interspherulitic porosity of the material at the expense of its mechanical properties. Therefore, trade-offs need to be made depending on the targeted applications. Based on the results from the established phase diagram and the SEM images, it is now possible to determine the location of PEG within the PLLA microstructure depending on the temperature of the isotherms. The different possible morphologies of the PLLA/PEG blends are presented in Figure 8, where PEG is represented in blue and PLLA in gray. In the high-temperature regime, the blend is in the liquid phase, where PEG and PLLA form a homogeneous liquid (type I) resulting in a single phase (Figure 8a), or form a liquid–liquid phase-separated mixture (type IV) with a PEG-rich phase and a PLLA-rich phase (Figure 8b). However, in the low-temperature regime, the crystallization of PLLA in the presence of liquid PEG needs to be considered using Keith and Padden's theory.[7] Therefore, when PLLA crystallizes (type II and III) slowly (radial growth G decreases), PEG has enough time to diffuse out of the spherulites, and the segregation spatial scale δ is large,

https://doi.org/10.1021/acsapm.4c01509
ACS Appl. Polym. Mater. 2024, 6, 9160–9169

corresponding to the presence of interspherulitic PEG regions (Figure 8c). However, if the crystallization rate G is larger than the diffusion coefficient D, a larger proportion of PEG is trapped inside the spherulites either in interlamellar (Figure 8e) or interfibrillar regions (Figure 8d). In the case of interlamellar segregation, amorphous interlamellar regions exist in which the PLLA and PEG chains are mixed; in this case, complete PEG extraction might be difficult and the porosity might be difficult to detect.

CONCLUSIONS

In this study, the thermal behavior of PLLA and PEG blends of different compositions was examined, focusing on the phase diagram and the potential for induced porosity. Thermal analysis was performed with fDSC in order to quench the structure of the blend after 5 min of equilibration time; it revealed four distinct blend behaviors. Above ca. 130 °C, no crystallization occurs and PLLA and PEG form a homogeneous liquid (type-I behavior) at 10% PEG content; for higher PEG contents, type-IV behavior was observed with liquid−liquid phase separation due to the presence of an LCST. For the higher molar mass PEG, the possible existence of a UCST was also detected. Below ca. 130 °C, type-II behavior was seen at lower PEG concentrations, in which PLLA crystallization induced liquid−solid phase separation with the interlamellar and possibly some interfibrillar segregation of PEG. For larger PEG amounts, type-III behavior emerged, with PLLA crystallization resulting in the segregation of PEG in larger regions located between lamellar stacks or between spherulites of the PLLA microstructure. The proportion of interspherulitically segregated PEG increases with PEG concentration and for decreasing PEG molar mass, in accordance with predictions of Keith and Padden. Temperature−concentration phase diagrams were then drawn for different PEG molecular masses. Although the composition has a large impact on PLLA/PEG miscibility and phase separation, the effect of the PEG molar mass mostly influences the transitions from one state to another.

Moreover, the present work allows one to showcase the induced porosity in the PLLA/PEG blends after PEG extraction with water. SEM images, both at the surface and in the core of the porous films, revealed that the PEG molar mass influences the proportion of PEG expelled from the PLLA spherulites and therefore the interspherulitic porosity, whereas intraspherulitic porosity looks identical regardless of the PEG molar mass. In contrast, the composition plays a major role in the final porosity. For instance, 90/10 blends show almost no porosity, whereas 50/50 blends were so porous that they were extremely brittle. Therefore, 70/30 blends made of PEG of high molar mass are the most promising ones to reach a high porosity while keeping reasonable mechanical properties for the material.

Overall, this research work offers insights into the development of porous materials with controlled hierarchical structures through a fine understanding of the PLLA/PEG phase diagram and selective PEG extraction from PLLA/PEG blends. This technique could be further combined with another method to create porosity, such as 3D printing, to obtain samples displaying different levels of porosity, which could serve as a foundation for designing materials with precise properties, including porosity, especially in the context of biomedical applications such as for bone tissue regeneration.

ASSOCIATED CONTENT

Supporting Information

The Supporting Information is available free of charge at https://pubs.acs.org/doi/10.1021/acsapm.4c01509.

Effect of isothermal treatment duration for PLLA/PEG 1M 50/50 and PLLA/PEG 3K 50/50; fDSC curves of pure PLLA; fDSC curves of pure PEG 3K, 100K, and 1M; enthalpies of melting for PLLA and PEG extracted from Figure 2; and ^{1}H NMR spectra of PLLA/PEG 100K 70/30 before and after extraction (PDF)

AUTHOR INFORMATION

Corresponding Author

Quentin Papeloer − *Institute of Condensed Matter and Nanosciences, UCLouvain, Louvain-la-Neuve 1348, Belgium;* orcid.org/0009-0008-6487-2955; Email: quentin.papeloer@uclouvain.be

Authors

Pascal Van Velthem − *Institute of Condensed Matter and Nanosciences, UCLouvain, Louvain-la-Neuve 1348, Belgium;* orcid.org/0000-0002-9998-5406

Sophie Demoustier-Champagne − *Institute of Condensed Matter and Nanosciences, UCLouvain, Louvain-la-Neuve 1348, Belgium;* orcid.org/0000-0003-3045-6060

Alain M. Jonas − *Institute of Condensed Matter and Nanosciences, UCLouvain, Louvain-la-Neuve 1348, Belgium;* orcid.org/0000-0002-4083-0688

Complete contact information is available at: https://pubs.acs.org/10.1021/acsapm.4c01509

Notes

The authors declare no competing financial interest.

REFERENCES

(1) Woodard, J. R.; Hilldore, A. J.; Lan, S. K.; Parc, C. J.; Morgan, A. W.; Eurell, J. A. C.; Clark, S. G.; Wheeler, M. B.; Jamison, R. D.; Wagoner Johnson, A. J. The mechanical properties and osteoconductivity of hydroxyapatite bone scaffolds with multi-scale porosity. *Biomaterials* **2007**, *28* (1), 45−54.

(2) Karageorgiou, V.; Kaplan, D. Porosity of 3D biomaterial scaffolds and osteogenesis. *Biomaterials* **2005**, *26* (27), 5474−5491.

(3) Loh, Q. L.; Choong, C. Three-dimensional scaffolds for tissue engineering applications: Role of porosity and pore size. *Tissue Eng., Part B* **2013**, *19* (6), 485−502.

(4) Jeyachandran, D.; Cerruti, M. Glass, Ceramic, Polymeric, and Composite Scaffolds with Multiscale Porosity for Bone Tissue Engineering. *Adv. Eng. Mater.* **2023**, *25* (17), 2201743.

(5) Premkumar, J.; Sonicasree, K.; Sudhakar, T. Polymers in Biomedical Use. *Handbook of Polymer and Ceramic Nanotechnology*; Springer, 2021; pp 1−28.

(6) Saini, P.; Arora, M.; Kumar, M. N. V. R. Poly(lactic acid) blends in biomedical applications. *Adv. Drug Delivery Rev.* **2016**, *107*, 47−59.

(7) Keith, H. D.; Padden, F. J. A Phenomenological Theory of Spherulitic Crystallization. *J. Appl. Phys.* **1963**, *34*, 2409−2421.

(8) Younes, H.; Cohn, D. Phase separation in Poly(ethylene glycol)/Poly(Lactic acid) blends. *Eur. Polym. J.* **1988**, *24* (8), 765−773.

(9) Sheth, M.; Kumar, R. A.; Davé, V.; Gross, R. A.; McCarthy, S. P. Biodegradable Polymer Blends of Poly (lactic acid) and Poly (ethylene glycol). *J. Appl. Polym. Sci.* **1997**, *66*, 1495−1505.

(10) Wang, B.; Hina, K.; Zou, H.; Zuo, D.; Yi, C. Thermal, crystallization, mechanical and decomposition properties of poly-(lactic acid) plasticized with poly(ethylene glycol). *J. Vinyl Addit. Technol.* **2018**, *24*, E154−E163.

(11) Li, F. J.; Zhang, S. D.; Liang, J. Z.; Wang, J. Z. Effect of polyethylene glycol on the crystallization and impact properties of polylactide-based blends. *Polym. Adv. Technol.* **2015**, *26* (5), 465−475.
(12) Nakafuku, C.; Sakoda, M. Melting and crystallization of poly(l-lactic acid) and poly(ethylene oxide) binary mixture. *Polym. J.* **1993**, *25* (9), 909−917.
(13) Nakafuku, C. Effects of molecular weight on the melting and crystallization of poly(L-lactic acid) in a mixture with poly(ethylene oxide). *Polym. J.* **1996**, *28* (7), 568−575.
(14) Zhang, Y.; Wang, Z.; Jiang, F.; Bai, J.; Wang, Z. Effect of miscibility on spherulitic growth rate for double-layer polymer films. *Soft Matter* **2013**, *9* (24), 5771−5778.
(15) Agari, Y.; Sakai, K.; Kano, Y.; Nomura, R. Preparation and Properties of the Biodegradable Graded Blend of Poly(L-lactic acid) and Poly(ethylene oxide). *J. Polym. Sci., Part B: Polym. Phys.* **2007**, *45*, 2972−2981.
(16) Tsuji, H.; Smith, R.; Bonfield, W.; Ikada, Y. Porous biodegradable polyesters. I. Preparation of porous poly(L-lactide) films by extraction of poly(ethylene oxide) from their blends. *J. Appl. Polym. Sci.* **2000**, *75* (5), 629−637.
(17) Nakane, K.; Hata, Y.; Morita, K.; Ogihara, T.; Ogata, N. Porous poly(L-lactic acid)/poly(ethylene glycol) blend films. *J. Appl. Polym. Sci.* **2004**, *94* (3), 965−970.
(18) Selvam, S.; Chang, W. V.; Nakamura, T.; Samant, D. M.; Thomas, P. B.; Trousdale, M. D.; Mircheff, A. K.; Schechter, J. E.; Yiu, S. C. Microporous Poly(L-Lactic Acid) Membranes Fabricated by Polyethylene Glycol Solvent-Cast/Particulate Leaching Technique. *Tissue Eng., Part C* **2009**, *15* (3), 463−474.
(19) Sun, X.; Xue, B.; Tian, Y.; Qin, S.; Xie, L. 3D porous poly(L-lactic acid) materials with controllable multi-scale microstructures and their potential application in oil-water separation. *Appl. Surf. Sci.* **2018**, *462*, 633−640.
(20) Reignier, J.; Huneault, M. A. Preparation of interconnected poly(ε-caprolactone) porous scaffolds by a combination of polymer and salt particulate leaching. *Polymer* **2006**, *47* (13), 4703−4717.
(21) Huang, R.; Zhu, X.; Tu, H.; Wan, A. The crystallization behavior of porous poly (lactic acid) prepared by modi fi ed solvent casting/particulate leaching technique for potential use of tissue engineering scaffold. *Mater. Lett.* **2014**, *136*, 126−129.
(22) Xu, Y.; Yu, W.; Zhou, C. Liquid-liquid phase separation and its effect on the crystallization in polylactic acid/poly(ethylene glycol) blends. *RSC Adv.* **2014**, *4* (98), 55435−55444.
(23) Fox, T. G. Influence of Diluent and of Copolymer Composition on the Glass Temperature of a Polymer System. *Bull. Am. Phys. Soc.* **1956**, *1*, 123.
(24) Hoffman, J. D.; Weeks, J. Melting Process and the Equilibrium Melting Temperature of Polychlorotrifluoroethylene. *J. Res. Natl. Bur. Stand. A Phys. Chem.* **1962**, *66A*, 13.
(25) Pyda, M.; Bopp, R. C.; Wunderlich, B. Heat capacity of poly(lactic acid). *J. Chem. Thermodyn.* **2004**, *36* (9), 731−742.
(26) Brandrup, J.; Immergut, E. H. *Polymer Handbook*, 3rd ed.; John Wiley, 1989.
(27) Couchman, P. R. Compositional Variation of Glass-Transition Temperatures. 2. Application of the Thermodynamic Theory to Compatible Polymer Blends. *Macromolecules* **1978**, *11* (6), 1156−1161.
(28) Jonas, A. M.; Ivanov, D. A.; Yoon, D. Y. The semicrystalline morphology of poly(ether-ether-ketone) blends with poly(ether-imide). *Macromolecules* **1998**, *31* (16), 5352−5362.
(29) Lai, W. C.; Bin Liau, W.; Yang, L. Y. Preparation of porous biodegradable PLLA with tunable pore size through simple variation of PEG/PLLA-blend crystallization conditions. *Polym. Adv. Technol.* **2023**, *34* (1), 398−404.

https://doi.org/10.1021/acsapm.4c01509
ACS Appl. Polym. Mater. 2024, 6, 9160−9169